exo-SUBSTITUENT EFFECTS IN HALOGENATED ICOSAHEDRAL ($B_{12}H_{12}^{2-}$) AND OCTAHEDRAL ($B_6H_6^{2-}$) *closo*-BORANE SKELETONS: CHEMICAL REACTIVITY STUDIED BY EXPERIMENTAL AND QUANTUM CHEMICAL METHODS

Martin LEPŠÍK[a1], Martin SRNEC[a2], Drahomír HNYK[b1], Bohumír GRÜNER[b2], Jaromír PLEŠEK[b3], Zdeněk HAVLAS[a3] and Lubomír RULÍŠEK[a4,*]

[a] *Institute of Organic Chemistry and Biochemistry, Academy of Sciences of the Czech Republic, v.v.i., Gilead Sciences Research Center & IOCB, Flemingovo nám. 2, 166 10 Prague 6, Czech Republic; e-mail: [1] lepsik@uochb.cas.cz, [2] srnec@uochb.cas.cz, [3] havlas@uochb.cas.cz, [4] lubos@uochb.cas.cz*

[b] *Institute of Inorganic Chemistry, Academy of Sciences of the Czech Republic, v.v.i., Husinec-Řež 1001, 250 68 Řež, Czech Republic; e-mail: [1]hnyk@iic.cas.cz, [2] gruner@iic.cas.cz, [3] plesek@iic.cas.cz*

Received September 24, 2008
Accepted November 6, 2008
Published online January 13, 2009

Dedicated to the memory of Professor Otto Exner.

The *exo*-substituent effects in halogenated icosahedral $B_{12}H_{12}^{2-}$ (**B12**) and octahedral $B_6H_6^{2-}$ (**B6**) *closo*-borane skeletons were studied both experimentally and theoretically. Firstly, the equilibrium geometries of *exo*-substituted **B12** and **B6** clusters were obtained using quantum chemical calculations at the MP2/def2-SVP level. A comparison with the available X-ray crystallographic data revealed a very good agreement between the theoretical and experimental values. Secondly, other descriptors of the molecular structure of these borane compounds – ^{11}B NMR chemical shifts – were experimentally determined and compared with the calculated values obtained by the *ab initio*/GIAO approach at the MP2/def2-TZVP level. It was shown that the calculated data reproduced the experiment very closely. Thirdly, we investigated experimentally the halogenation reactions of **B12** and attempted to explain the observed ratios between the two obtained disubstituted products (*meta*/*ortho* ~ 4:1) by calculating their thermodynamic stabilities using the DFT/B3LYP method. These calculations showed the enhanced stability of the *meta* disubstituted **B12** but did not explain why the *para* product had not been observed in the experiment. We thus turned our attention to the kinetic aspects of *exo*-substitution reactions by exploring the possible reaction pathways and transition states. In spite of the complexity of the plausible reaction mechanisms, reasonable agreement was obtained between the calculated activation barriers and the experimental observations concerning the halogenation reactions of the **B6** and **B12** molecules. It also allowed to exclude from considerations certain reaction pathways leading to the mono- and dihalogenated **B12** and **B6** species.

Keywords: Boranes; Boron clusters; Halogenations; DFT; Ab initio calculations; Reaction mechanism; Substituent effects.

doi:10.1135/cccc2008189

Icosahedral dodecaborate ($B_{12}H_{12}^{2-}$, **B12**, Fig. 1a) and octahedral hexaborate ($B_6H_6^{2-}$, **B6**, Fig. 1b) belong to the most stable and the most symmetrical skeletons in the whole boron hydride chemistry and are often used as references for the quantitative comparison of the stabilities of other *closo*-clusters (see ref.[1]). Structurally, these parent compounds of deltahedral *closo*-borane dianions $B_nH_n^{2-}$ (n = 5–12) belong to the O_h and I_h point groups of symmetry, respectively, which is reflected in their perfectly symmetrical delocalized deltahedral bonding. All the triangular boron facets are thus regular and equal. The nature of the bonding in these clusters is determined by the electron-deficiency of boron atoms which are mostly involved in three-centre-two-electron (3c2e) bonds[2].

Since the ^{11}B isotope is NMR-active (it has a nuclear spin I = 3/2), the three-dimensional structures of polyhedral boranes can be deduced from NMR spectroscopy experiments[3]. As a theoretical complement, ^{11}B chemical shifts – $\delta(^{11}B)$, which are extremely sensitive to changes in structure, can be calculated using the so-called *ab initio*/GIAO(IGLO)/NMR method[4]. This computational tool has been widely used in boron cluster chemistry and quickly approaches a confidence level that rivals that of modern X-ray analysis[5].

Experimental boron chemists have been studying the substitution chemistry of **B12** and **B6** cages, i.e. the replacement of one or more exoskeletal hydrogens with various atoms or functional groups, for several decades (reviewed in ref.[6] for **B12** and ref.[7] for **B6**). Despite the abundance of experimental knowledge on the *exo*-substituent derivatives of **B12** and **B6**, the

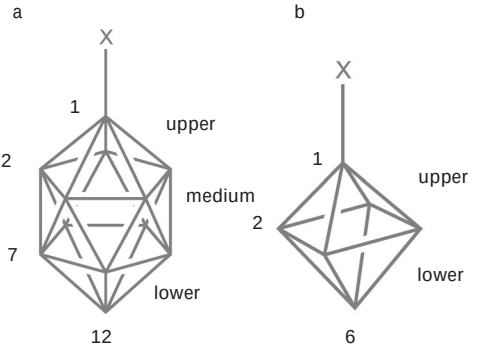

FIG. 1
The schematic structure (each vertex standing for a BH group), boron atom numbering and position of the upper, (medium), and lower belts in the a $B_{12}H_{11}X^{2-}$ (**B12**) and b $B_6H_5X^{2-}$ (**B6**) systems

observed directive effects of the substituents for further substitution at other sites of the cage have still eluded a mechanistic understanding[6–8].

In order to investigate these effects, we have focused in this study on the mono- and dihalogenated $B_{12}H_{12-n}X_n^{2-}$ or $B_6H_{6-n}X_n^{2-}$ species, where (X = F, Cl, Br and n = 1, 2), with the positional isomers of the dihalogenated species being further denoted as *ortho* (1,2-$B_{12}H_{10}X_2^{2-}$), *meta* (1,7-$B_{12}H_{10}X_2^{2-}$) and *para* (1,12-$B_{12}H_{10}X_2^{2-}$) for **B12**, and *cis* (1,2-$B_6H_4X_2^{2-}$) and *trans* (1,6-$B_6H_4X_2^{2-}$) for **B6** [9].

In the first part, we will present the experimental data on the halogenation reactions of **B12** along with the results from ^{11}B NMR spectroscopy. Subsequently, we will investigate the electronic structure and equilibrium geometries, ^{11}B NMR chemical shifts, the stability, and halogenation reactions of the **B12** and **B6** skeletons using quantum chemical (QM) calculations. In the end, we will draw, based on both the experimental and theoretical data, conclusions concerning the directive effects of the halogen substituents on the **B12** and **B6** cages. A comparison will be made with the aromatic organic systems, such as the benzene molecule, as other representatives of structures with highly delocalized electronic distribution. For these, the substituent effects are well-known and have also been studied theoretically in great depth by Exner and Böhm[10–14]. Furthermore, the geometrical consequences of benzene ring *exo*-substitutions have been carefully examined by Domenicano[15], and this approach has been applied to *exo*-substitutions in the *closo*-1,12-$C_2B_{10}H_{12}$ cluster, i.e. in the icosahedral skeleton with a lower symmetry than for $B_{12}H_{12}^{2-}$ due to its 1,12-vertex substitutions[16].

EXPERIMENTAL

Instrumental Techniques

^{1}H and ^{11}B NMR spectroscopy investigations were performed on a Varian Mercury 400 Plus Instrument at 298 K in deuterioacetone as the solvent. The NMR chemical shifts (δ-scale) are given in ppm to the high frequency (low field) with respect to $BF_3{\cdot}OEt_2$ (0.0 ppm). The spectra were measured with $B(OMe)_3$ in a glass capillary as the internal reference (18.1 ppm). The coupling constants $^1J(^{11}B\text{-}^1H)$ are given in Hz and are taken from the resolution-enhanced ^{11}B spectra with a digital resolution of 2 Hz. The NMR data presented in the text below are in the following format: ^{11}B NMR: ^{11}B chemical shifts, $\delta(^{11}B)$ in ppm, multiplicity, coupling constants $J(^{11}B\text{-}^1H)$ in Hz. Peak assignment is based on the $^{11}B\text{-}^{11}B$ COSY spectra with the full assignment of crosspeaks.

The mass spectrometry measurements were performed on a Thermo-Finnigan LCQ-Fleet Ion Trap instrument using electrospray ionization (ESI). Negative ions were detected. The samples dissolved in acetonitrile (concentrations of approximately 100 ng ml^{-1}) were intro-

duced to the ion source by the infusion of 0.25 ml h^{-1}. The instrument setup was as follows: source voltage at 5.98 kV, tube lens voltage at –74.8 V, capillary voltage at –35.05 V, gate lens voltage at 53.96 V, a drying temperature of 180 °C, a drying gas flow of 6 l min^{-1}, and auxiliary gas pressure of 6 bar. In all the cases, dinegative ions corresponding to the molecular ion were observed and, with the exception of 1,7-$B_{12}H_{10}F_2^{2-}$, showing $[M]^{2-}$ as the most abundant peak, the base peaks observed with 100% abundance corresponded to a $[M + Bu_4N^+]^-$ monovalent complex containing one Bu_4N^+ cation. Full agreement of the experimental and calculated isotopic distribution pattern was observed for all these compounds. The isotopic distribution in the boron plot of the $[M]^{2-}$ peaks is in agreement with the charge, showing distances of 1/2 mass units for the dianionic compounds.

Isolation of the Individual Isomers

The products of the halogenation reactions were separated on a preparative scale using commercially available ion-exchange DEAE pearl cellulose OSTSORB (Spolchemie, Ústí nad Labem, Czech Republic). The use of this cellulose, characterized by hydrophilic backbone, spherical particles, rather narrow particle size distribution (100 μm), ion exchange capacity (0.5 meq g^{-1}) and very good flow properties, made it possible to achieve quite efficient separation of the isomers and the isolation of both the pure 1,7-$B_{12}H_{10}X_2^{2-}$ and the 1,2-$B_{12}H_{10}X_2^{2-}$ series, except for fluoro derivative, where only 1,7-$B_{12}H_{10}F_2^{2-}$ was isolated. The $B_{12}H_{10}X_2^{2-}$ (X = Cl, Br) derivatives were eluted using 1 M ammonium nitrate, while 0.5 M ammonium chloride was used for the less retained $B_{12}H_{10}F_2^{2-}$ derivatives. The eluted compounds were precipitated off the aqueous buffer by the excess Bu_4NCl aqueous solution and recovered by filtration. The product composition and purity of the fractions from the preparative chromatography (after precipitation and conversion to conjugated acids by ion exchange) were analysed using the published HPLC method[17], designed particularly for the separation of the hydrophobic divalent boron cluster anions (Scheme 1).

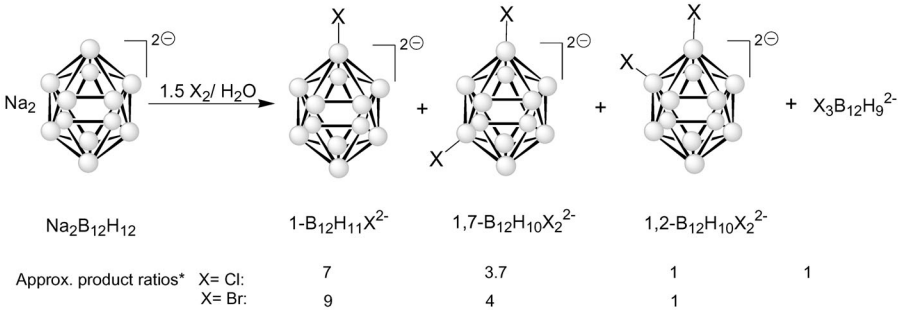

SCHEME 1

The main products formed by the titration of $Na_2B_{12}H_{12}$ with 1.5 equivalents of Cl_2 and Br_2. The product ratios are based on an HPLC analysis of the product composition while neglecting the changes in their UV absorbance. Under these conditions, unreacted $B_{12}H_{12}^{2-}$ and, in case of chlorination, also minor quantities of several isomers of $B_{12}H_9Cl_3^{2-}$ derivatives are present in the reaction mixture

Fluorination. $K_2B_{12}H_{12}$ (0.5 g) was gained from high-purity triethyl ammonium salt by a similar conversion as was used for the sodium salts (see below for chlorination). The salt was dried at 110 °C for 8 h in vacuum in a Teflon™ flask. The flask was subsequently cooled in a bath to –70 °C, after which HF in excess (2 ml) was condensed into it from a steel container under a stream of dry nitrogen. The flask was then closed and left to stand at –20 °C for 48 h. The flask was subsequently opened in the hood, and the excess HF was left to fume out. The product mixture was dissolved in H_2O (5 ml) and separated on the DEAE cellulose column (78 × 2.1 cm) in a way similar to what was described above, but using 0.5 M NH_4Cl as the mobile phase. A peak with an elution volume *V* (in l): 1,7-$B_{12}H_{10}F_2^{2-}$ (1.51–1.65) was collected. The elution was monitored by the HPLC method (a Column Separon HEMA Bio 300 (7 μm, hydroxyethyl methacrylate) 150 × 3 mm ID, 0.5 M $NaClO_4$ as the mobile phase, a flow rate of 0.5 ml min^{-1}, detection UV 200 nm) by direct injections of the effluent from the preparative column. The respective collected fraction was treated as described below for the $B_{12}H_{10}Cl_2^{2-}$ derivatives. Data used for compounds characterization: ^{11}B NMR (128 MHz, acetone-d_6), $(Bu_4N)_2$[1,7-$F_2B_{12}H_{10}$]: 6.6 (s, B1,7); –18.1 (d, B2,3); –19.5 (d, B4,6,8,11); –21.7 (d, *J* = 124, B9,10); –25.4 (d, *J* = 134, B5,12). MS (ESI), *m/z*, $(Bu_4N)_2$[1,7-$F_2B_{12}H_{10}$]: 90.33 (100%) $[M]^{2-}$, calculated 90.09; 422.47 (10%) $[M + Bu_4N^+]^-$, calculated 422.47.

Chlorination. In a typical experiment, a suspension of the $(Et_3NH)_2B_{12}H_{12}$ (0.99 g, 2.86 mmol) of high purity (>99.5% HPLC and ^{11}B NMR check) in water (50 ml) was converted to hydrated sodium salt by the addition of 1.0 M NaOH (5.9 ml, 5.72 mmol) and evaporation in vacuum at 50 °C. The hydrated salt was dissolved in water (100 ml) and then cooled down to 0 °C under stirring. Subsequently, a steel pressure bottle containing a previously prepared and analysed (iodometric titration) mixture of chlorine in nitrogen (62 mg of Cl_2 in 1 l) was attached and the gas was bubbled through the stirred solution at a velocity of 1.5 l h^{-1}. The gas volume (5.0 l) was measured by a laboratory gas gauge (connected through a wash bottle containing 30 ml of a 0.1 M solution of KI and 1 ml of a starch solution as an indicator) with a precision of 0.1 l. The chlorine was consumed quantitatively as verified by an iodometric titration of the content of the wash bottle (containing 0.1 M KI) by 0.2 M $Na_2S_2O_3$. The course of the chlorination was also monitored by the HPLC method. When 1.5 equivalents of Cl_2 were introduced, the solution was stirred for an additional 1 h, after which nitrogen gas was bubbled through the flask for 30 min. The ratios of the individual derivatives and isomers present in the reaction mixture, as determined by an HPLC analysis[17] (neglecting the differences in UV absorbance for the $B_{12}H_{10}Cl_2^{2-}$ derivatives), were 4:7:1:3.7:1 for $B_{12}H_{12}^{2-}$, $B_{12}H_{11}Cl^{2-}$, 1,2-$Cl_2B_{12}H_{10}^{2-}$, 1,7-$Cl_2B_{12}H_{10}^{2-}$ and $B_{12}H_9Cl_3^{2-}$. Aqueous phase (70 ml) was taken and the water was removed in vacuum to dryness. The solid was dissolved in water (5 ml) and injected on top of a freshly prepared column (73 × 2.1 cm ID) with DEAE pearl cellulose OSTSORB (350 ml of swollen cellulose, a particle size of 100 μm, an ion exchange capacity of ca. 0.5 mequiv/ml), which had been cycled several times between 0.1 M NaOH and 0.1 M HCl, washed with water, then filled into the column, and equilibrated with 1.0 M NH_4NO_3. The respective compounds were eluted by 1.0 M NH_4NO_3 at a flow rate of approximately 5 ml min^{-1}, and the following fractions with elution volume *V* (in l) were collected: unreacted $B_{12}H_{12}^{2-}$ (0.8–0.9), 1-$ClB_{12}H_{11}^{2-}$ (1.0–1.15), 1,2-$Cl_2B_{12}H_{10}^{2-}$ (1.25–1.45), 1,7-$Cl_2B_{12}H_{10}^{2-}$ (1.65–1.90) followed by small amounts of 1,2,3- and 1,7,9-$Cl_3B_{12}H_9^{2-}$ isomers and other $Cl_3B_{12}H_9^{2-}$ derivatives. Aqueous Bu_4NCl was added to the respective fractions and the resulting precipitate was left to stand for 3 h and then filtered off by a dense pore glass filter. The products were washed with water and dried in the air and in vacuum. Data used for compounds characterization: ^{11}B NMR (128 MHz,

acetone-d_6), $(Bu_4N)_2$ 1: –15.32 (d, J = 125, B1–12); $(Bu_4N)_2[1\text{-}ClB_{12}H_{11}]$: –2.8 (s, B1), –14.8 (d, J = 130, B2–5), –16.6 (d, J = 128, B7–11), –20.2 (d, J = 127, B12); $(Bu_4N)_2[1,2\text{-}Cl_2B_{12}H_{10}]$: –3.7 (s, B1,2), –13.8 (d, J = 123, B3,6), –15.3 (d, J = 132.1, B4,5,7,11), –18.1 (d, J = 134, B8,10), –20.1 (d, J = 130, B9,12); $(Bu_4N)_2[1,7\text{-}Cl_2B_{12}H_{10}]$: –3.7 (s, B1,7), –13.8 (d, J = 124, B2,3), –15.4 (d, J = 133, B4,6,8,11), –17.5 (d, J = 124, B9,10), –19.2 (d, J = 134, B5,12). MS (ESI), *m/z*, $(Bu_4N)_2[1\text{-}ClB_{12}H_{11}]$: 90.08 (65%) $[M]^{2-}$, calculated 90.08; 420.46 (100%) $[M + Bu_4N^+]^-$, calculated 420.45; $(Bu_4N)_2[1,2\text{-}Cl_2B_{12}H_{10}]$: 107.74 (55%) $[M]^{2-}$, calculated 107.56; 458.42 (100%) $[M + Bu_4N^+]^-$, calculated 458.41; $(Bu_4N)_2[1,7\text{-}Cl_2B_{12}H_{10}]$: 107.56 (55%) $[M]^{2-}$, calculated 107.56; 458.41 (100%) $[M + Bu_4N^+]^-$, calculated 458.41.

Bromination. $(Et_3NH)_2B_{12}H_{12}$ (0.99 g, 2.86 mmol) was converted to hydrated sodium salt as described above for the $B_{12}H_{10}Cl_2^{2-}$ derivatives. The solid salt was dissolved in water (100 ml), and the solution was cooled down to 0 °C. Bromine (225 µl, 4.29 mmol) was injected into CCl_4 (60 ml) under shaking. This solution was slowly dropwise added (15 ml h^{-1}) to the stirred aqueous solution of $Na_2B_{12}H_{12}$. The ratios of the individual derivatives and isomers present in the reaction mixture, as determined by an HPLC analysis (neglecting the differences in UV absorbance for $B_{12}H_{10}Br_2^{2-}$ derivatives), were 1:9:1:4 for $B_{12}H_{12}^{2-}$, $1\text{-}BrB_{12}H_{11}^{2-}$, $1,2\text{-}Br_2B_{12}H_{10}^{2-}$ and $1,7\text{-}Br_2B_{12}H_{10}^{2-}$. Aqueous phase (70 ml) was taken and separated on the DEAE cellulose column (78 × 2.1 cm) in a similar way to the description above for the $B_{12}H_{10}Cl_2^{2-}$ derivatives. The following fractions with elution volume V (in l) were collected: $B_{12}H_{12}^{2-}$ (0.8–1.1), $1\text{-}BrB_{12}H_{11}^{2-}$ (1.50–1.75), $1,2\text{-}Br_2B_{12}H_{10}^{2-}$ (2.10–2.25), $1,7\text{-}Br_2B_{12}H_{10}^{2-}$ (2.35–2.60). The respective fractions were treated as above. Data used for compounds characterization: ^{11}B NMR (128 MHz, acetone-d_6), $(Bu_4N)_2[1\text{-}BrB_{12}H_{11}]$: –8.2 (s, B1), –14.3 (d, J = 134, B2–5), –15.9 (d, J = 127, B7–11), –18.9 (d, J = 130, B12); $(Bu_4N)_2[1,2\text{-}Br_2B_{12}H_{10}]$: –8.9 (s, B1,2), –13.3 (d, J = 156, B3,6), –14.7 (d, J = 135, B4,5,7,11), –16.9 (d, J = 155, B8,10), –18.7 (d, J = 124, B9,12); $(Bu_4N)_2[1,7\text{-}Br_2B_{12}H_{10}]$: –9.0 (s, B1,7), –13.4 (d, J = 156, B2,3), –14.6 (d, J = 150, B4,6,8,11), –16.2 (d, J = 126, B9,10), –17.9 (d, J = 150, B5,12). MS (ESI), *m/z*, $(Bu_4N)_2[1\text{-}BrB_{12}H_{11}]$: 112.05 (20%) $[M]^{2-}$, calculated 112.06; 466.40 (100%) $[M + Bu_4N^+]^-$, calculated 466.40; $(Bu_4N)_2[1,2\text{-}Br_2B_{12}H_{10}]$: 152.67 (15%) $[M + H]^-$, calculated 152.51; 546.18 (100%) $[M + Bu_4N^+]^-$, calculated 546.31; $(Bu_4N)_2[1,7\text{-}Br_2B_{12}H_{10}]$: 305.06 (30%) $[M + H]^-$, calculated 305.03; 546.22 (100%) $[M + Bu_4N^+]^-$, calculated 546.31.

COMPUTATIONAL DETAILS

The density functional theory (DFT) and Møller–Plesset (MP2) calculations reported in the study were carried out using the Turbomole 5.10 [18] and Gaussian 03 [19] programs. For DFT, the Perdew–Burke–Ernzerhof (PBE)[20] and hybrid three-parameter Becke's (B3LYP)[21] functionals were used throughout. The calculations were expedited by expanding the Coulomb integrals in an auxiliary basis set, the so-called resolution-of-identity (RI-J) approximation in Turbomole[22,23] or density fitting in Gaussian. All the geometry optimizations were carried out using a double-ζ basis set, the def2-SVP basis set[24,25]. The single-point energies were recomputed in a larger triple-ζ basis set, denoted def2-TZVP (triple-ζ valence with two polarization functions on each atom)[26] in Turbomole.

The solvation effects were taken into account using the COSMO method[27,28] at the RI-PBE/def2-SVP level with the dielectric constants ε_r = 83.6 for liquid anhydrous hydrogen fluoride (LAHF)[29] and ε_r = 80 for water. As the standard option, we used the Bondi atomic radii multiplied by 1.17. The total Gibbs free energy of a molecule was calculated as the sum of the following contributions:

$$G = E_{el} + G_{solv} + E_{ZPE} - RT \ln (q_{trans}\, q_{rot}\, q_{vib}) \quad (1)$$

where E_{el} is the gas-phase energy of the system (at the B3LYP/def2-TZVP level and the geometry optimized at the RI-PBE/def2-SVP level), G_{solv} is the solvation free energy, E_{ZPE} is the zero-point energy, and $-RT \ln (q_{trans}\, q_{rot}\, q_{vib})$ accounts for the entropic terms and the thermal correction to the enthalpy obtained from a calculation of analytical harmonic vibrational frequencies using the same method and software as for the geometry optimizations at the RI-PBE/def2-SVP level, 298 K and 1 atm, using the ideal-gas approximation[30].

The NMR shieldings (σ_{calc}) of the substituted **B12** or **B6** compounds (see Eq. (*2*)) were calculated using the gauge-including atomic orbital many-body second-order perturbation (GIAO-MBPT(2)) method[31] implemented in the Turbomole package. Two levels of theory, the coupled perturbed Hartree-Fock (CPHF)[32] or Møller–Plesset (MP2) method, were used. Two basis sets, namely the def2-SVP and def2-TZVP (for details, see above) were combined with either of the two above-mentioned methods. ^{11}B chemical shifts – $\delta(^{11}B)$ – were calculated relative to diborane (B_2H_6) and converted to the standard $BF_3{\cdot}OEt_2$ scale by using an experimental $\delta(^{11}B)$ value of diborane of 16.6 ppm (Eq. (*2*))[33]. The σ_{calc}(diborane) values computed at the HF/def2-SVP, MP2/def2-SVP, HF/def2-TZVP and MP2/def2-TZVP levels were 106.8, 104.4, 100.3 and 95.8 ppm, respectively.

$$\delta(^{11}B) = \delta(^{11}B)_{B2H6} + \sigma_{calc}(B_2H_6) - \sigma_{calc} \quad (2)$$

The transition states of the reactions were searched starting either from estimates based on chemical intuition or in analogy with the work of McKee[34] or using a relaxed energy scan of the incipient B–X distance (1.4–4.7 Å). These estimates were further refined by a diagonalization of the Hessian matrix using the AOFORCE module in Turbomole 5.10 and optimizations along the selected transition vectors. The relevancy of a located transition state was confirmed by determining a single imaginary

vibrational frequency of a transition vector, which pointed in the direction of the reaction pathway.

RESULTS

*The Geometrical Effects of exo-Substitutions on **B12** and **B6** Skeletons*

The selected parameters describing the equilibrium geometries of the parent and *exo*-substituted **B12** and **B6** skeletons obtained by optimization at the MP2/def2-SVP level are shown in Table I. The growing size of the substituent, manifested in the increasing B1–X (X = H, F, Cl, Br) distances, causes a small shrinkage of the remaining distances in the **B12** and **B6** cages (on the order of hundredths of Å). This effect is most pronounced for the B1–B6 distance in **B6** cages (cf. $R_{(B1–B6)}$ = 2.47 Å in $B_6H_6^{2-}$ and $R_{(B1–B6)}$ = 2.39 Å in 1,6-$Br_2B_6H_4^{2-}$, see Table I).

By comparing the calculated equilibrium distances with the experimental values obtained from X-ray crystallography[35–37], it can be seen that reasonable overall agreement was obtained. The calculated B–B and B–X distances are usually slightly overestimated (up to 0.05 Å). The agreement is worse for B–H distances ($\Delta_{exp–calc}$ = 0.15 Å), because X–H distances obtained by X-ray crystallography have a slightly different physical meaning[38], which can also be demonstrated by comparing the calculated values with the experimental B–H bond length obtained from NMR spectroscopy on the polycrystalline $Cs_2B_6H_6$ compound ($R_{(B–H)}$ = 1.19 Å)[39] with $\Delta_{exp–calc}$ = 0.04 Å.

^{11}B NMR Chemical Shifts

Experimental Results

Fluorination. The assignment of peaks in the NMR spectrum of the pure 1,7-$B_{12}H_{10}F_2^{2-}$ isomer corresponds to that previously structurally characterized, but published without the NMR data[37b].

Chlorination and bromination. The availability of both series of pure isomers of $B_{12}H_{10}X_2^{2-}$ (X = Cl, Br) derivatives enabled the comparison of their ^{11}B NMR spectra and unequivocally assign the peaks from 128 MHz ^{11}B-^{11}B COSY NMR spectroscopy for both isomeric series as well as a comparison of the shifts with the spectra of the monosubstituted compounds. Indeed, the symmetry and the spectral pattern 2:2:4:2:2 is identical for the 1,7- and 1,2-series, and the differences in chemical shifts are relatively small. There

TABLE I

The equilibrium distances (in Å) in mono- and disubstituted **B12** and **B6** compounds obtained from MP2/def2-SVP optimizations. The corresponding values obtained by X-ray crystallography are shown in italics in parentheses

B12

X	Isomer	B1–X	B1–B2	B1–B7	B1–B12
H		1.22 *(1.10)*[a]	1.79 *(1.78)*[a]	2.90 *(2.89)*[a]	3.41 *(3.39)*[a]
F	mono	1.41	1.79	2.90	3.41
	ortho	1.41	1.80	2.90	3.41
	meta	1.41	1.79	2.91	3.41
	para	1.41	1.79	2.90	3.41
Cl	mono	1.85 *(1.84)*[b]	1.79 *(1.78)*[b]	2.89 *(2.87)*[b]	3.39 *(3.37)*[b]
	ortho	1.84	1.79	2.89	3.39
	meta	1.85	1.78	2.87	3.39
	para	1.85	1.79	2.88	3.38
Br	mono	2.02 *(2.02)*[b]	1.78 *(1.76)*[b]	2.88 *(2.85)*[b]	3.38 *(3.34)*[b]
	ortho	2.01	1.78	2.89	3.39
	meta	2.02	1.78	2.86	3.38
	para	2.02	1.78	2.88	3.36

B6

X	Isomer	B1–X	B1–B2	B1–B6
H		1.23 *(1.08)*[c]	1.75 *(1.72)*[c]	2.47 *(2.44)*[c]
F	mono	1.43	1.74	2.45
	cis	1.43	1.74	2.46
	trans	1.43	1.74	2.43
Cl	mono	1.87	1.73	2.44
	cis	1.86	1.73	2.45
	trans	1.87	1.73	2.41
Br	mono	2.05	1.73	2.42
	cis	2.03	1.72	2.44
	trans	2.03	1.73	2.39

[a] Ref.[35], [b] ref.[36], [c] ref.[37]

is no noticeable difference in the chemical shifts of the substituted atoms. The most profound difference has been found for the chemical shift of the signal of the antipodal atoms B(9,12) in 1,2-$B_{12}H_{10}Cl_2^{2-}$, which are shifted upfield (0.9 ppm) as compared to that of B(5,12) in the 1,7-isomer series. A similar upfield shift (0.8 ppm) has also been observed for the signal of antipodal atoms in the 1,2-$B_{12}H_{10}Br_2^{2-}$ derivative. The experimental data are listed in the Experimental and also provided in Table II along with the calculated values.

Theoretical Calculations

The calculated ^{11}B NMR chemical shifts for the *exo*-substituted **B12** and **B6** skeletons are summarized in Tables II and III. For the **B12** cages, the agreement with the experimental data is very good (~1–2 ppm per boron atom for triple-ζ basis sets and ~2–4 ppm for the double-ζ basis set, see Table S1 in Suplementary Material). For $B_{12}H_{10}Br_2^{2-}$ derivatives, the agreement is slightly worse for boron atoms with a bond to the bromine atom. In our opinion, this can be attributed to the neglect of an explicit treatment of the relativistic effects. We are aware that the inclusion of spin-orbit coupling might be necessary to obtain quantitatively accurate values of the ^{11}B chemical shifts for compounds containing heavier elements (Br, I) as has previously been shown for icosahedral 12-X-*closo*-1-$SB_{11}H_{10}X$ (X = F, Cl, Br, I) molecules[40]. For **B6** compounds, the agreement with experimental data was within 1–3 ppm except for $B_6H_5Cl^{2-}$ and $B_6H_5Br^{2-}$, where the calculated data deviated by ~5 ppm from the experimental values. However, it is also important to note the relatively large effect (up to 5 ppm for the $B_6H_6^{2-}$ molecule) of a counter ion present or solvent used in the experimental NMR setup[7].

In Table S1, we also present the values calculated using both the HF and MP2 methods and two sizes of the basis set (def2-SVP and def2-TZVP). It can be concluded that all the methods yield results of satisfactory accuracy with the mean average deviation (MAD) from the available experimental data being 1–5 ppm per boron atom.

The Stabilities of all the Positional Isomers of $B_{12}H_{10}X_2^{2-}$ and $B_6H_4X_2^{2-}$

The thermodynamic stabilities of all the positional isomers of dihalogenated (X = F, Cl, Br) **B12** (i.e. *ortho, meta, para*) and dihalogenated (X = Cl, Br) **B6** (i.e. *cis, trans*) compounds were evaluated using the DFT/B3LYP quantum chemical calculations (Table IV). The differences between the relative

TABLE II

The NMR chemical shifts (in ppm) for the **B12** molecules calculated at the MP2/def2-TZVP level and compared to the experimental values (where available)

Molecule	^{11}B NMR chemical shifts				
$B_{12}H_{12}^{2-}$	B1–12				
calcd.	–16.2				
exptl[a]	*–15.3*				
exptl[b]	*–14.4*				
$B_{12}H_{11}F^{2-}$	B1	B2–6	B7–11	B12	
calcd.	11.4	–17.1	–19.2	–26.0	
exptl[a]	*10.2*	*–16.7*	*–18.5*	*–24.0*	
exptl[b]	*9.8*	*–16.0*	*–17.6*	*–23.3*	
exptl[c]	*9.0*	*–16.7*	*–18.2*	*–23.9*	
1,2-$B_{12}H_{10}F_2^{2-}$	B1,2	B3,6	B4,5,7,8	B9,11	B10,12
calcd.	8.6	–18.5	–19.6	–23.4	–27.6
1,7-$B_{12}H_{10}F_2^{2-}$	B1,7	B2,6	B3,5,8,11	B4,12	B9,10
calcd.	9.0	–17.8	–19.9	–26.9	–22.4
exptl[a]	*6.6*	*–18.1*	*–19.5*	*–25.4*	*–21.7*
1,12-$B_{12}H_{10}F_2^{2-}$	B1,12	B2–11			
calcd.	8.3	–19.2			
$B_{12}H_{11}Cl^{2-}$	B1	B2–6	B7–11	B12	
calcd.	–0.7	–14.3	–16.8	–21.7	
exptl[a]	*–2.8*	*–14.8*	*–16.6*	*–20.2*	
1,2-$B_{12}H_{10}Cl_2^{2-}$	B1,2	B3,6	B4,5,7,8	B9,11	B10,12
calcd.	–1.5	–13.0	–14.8	–18.5	–21.3
exptl[a]	*–3.7*	*–13.8*	*–15.3*	*–18.3*	*–20.1*
1,7-$B_{12}H_{10}Cl_2^{2-}$	B1,7	B2,6	B3,5,8,11	B4,12	B9,10
calcd.	–1.2	–12.6	–15.0	–19.8	–17.5
exptl[a]	*–3.7*	*–13.8*	*–15.4*	*–19.2*	*–17.5*
1,12-$B_{12}H_{10}Cl_2^{2-}$	B1,12	B2–11			
calcd.	–2.6	–14.6			
$B_{12}H_{11}Br^{2-}$	B1	B2–6	B7–11	B12	
calcd.	–2.3	–13.9	–16.3	–20.6	
exptl[a]	*–8.2*	*–14.3*	*–15.9*	*–18.9*	
1,2-$B_{12}H_{10}Br_2^{2-}$	B1,2	B3,6	B4,5,7,8	B9,11	B10,12
calcd.	–2.8	–12.2	–13.9	–17.3	–19.9
exptl[a]	*–8.9*	*–13.3*	*–14.7*	*–16.9*	*–18.7*
1,7-$B_{12}H_{10}Br_2^{2-}$	B1,7	B2,6	B3,5,8,11	B4,12	B9,10
calcd.	–2.5	–11.9	–14.1	–18.3	–16.6
exptl[a]	*–9.0*	*–13.4*	*–14.6*	*–16.2*	*–17.9*
1,12-$B_{12}H_{10}Br_2^{2-}$	B1,12	B2–11			
calcd.	–3.4	–13.9			

[a] Refs[41,42], [b] ref.[43], [c] ref.[44]

TABLE III
The NMR chemical shifts (in ppm) for the **B6** molecules calculated at the MP2/def2-TZVP level and compared to the experimental values (where available)

Molecule	^{11}B NMR chemical shifts		
$B_6H_6^{2-}$	B1–6		
calcd.	–21.3		
exptl[a]	*–18.1; –13.2*		
$B_6H_5F^{2-}$	B1	B2–5	B6
calcd.	11.6	–24.5	–47.2
exptl[b]	*9.3*	*–17.1*	*–40.6*
1,2-$B_6H_4F_2^{2-}$	B1,2	B3,5	B4,6
calcd.	6.9	–28.3	–48.6
1,6-$B_6H_4F_2^{2-}$	B1,6	B2–5	
calcd.	1.5	–26.1	
$B_6H_5Cl^{2-}$	B1	B2–5	B6
calcd.	–3.2	–20.4	–35.9
exptl[a]	*–1.0*	*–14.5*	*–30.4*
1,2-$B_6H_4Cl_2^{2-}$	B1,2	B3,5	B4,6
calcd.	–4.8	–20.1	–33.6
exptl[a]	*–2.4*	*–15.4*	*–30.3*
1,6-$B_6H_4Cl_2^{2-}$	B1,6	B2–5	
calcd.	–10.0	–18.9	
exptl[a]	*–10.4*	*–13.6*	
$B_6H_5Br^{2-}$	B1	B2–5	B6
calcd.	–5.5	–19.5	–33.8
exptl[a]	*–7.6*	*–14.0*	*–27.3*
1,2-$B_6H_4Br_2^{2-}$	B1,2	B3,5	B4,6
calcd.	–6.5	–18.2	–30.4
exptl[a]	*–8.4*	*n/d*	*–26.9*
1,6-$B_6H_4Br_2^{2-}$	B1,6	B2–5	
calcd.	–11.0	–17.5	
exptl[a]	*–12.6*	*–15.0*	

[a] Ref.[45], [b] ref.[44]

stabilities of these isomers are quite small (up to 1 kcal mol^{-1}). In all cases, the *meta* disubstituted **B12** (or *cis* for **B6**) cages are predicted to be slightly more stable. It can be seen that the effects of the zero-point energy (ZPE) and entropic contributions (to obtain Gibbs free energy) as well as the inclusion of an implicit solvent are very small. The calculated thermodynamic stabilities correlate reasonably well with the observed positional preferences in the disubstituted **B12** cages predicting the *meta* isomer to be the most stable in all the cases. They also yield semi-quantitative agreement between the *ortho*/*meta* ratio (the calculated energy differences correspond to 1:3 to 1:5 for the three systems studied). Nevertheless, they do not explain why the *para* isomer is not observed. The experimental *cis*/*trans* ratio

TABLE IV
The calculated relative stabilities (in kcal mol^{-1}) of the dihalogenated **B12** and **B6** cages (the *meta* and *cis* isomers are taken as the reference)

		B12	
X	Isomer	$\Delta E_{\mathrm{B3LYP}}$ [a]	$\Delta G_{(\mathrm{aq})}$ [b]
F	*ortho*	0.6	**0.6**
	meta	0.0	**0.0**
	para	0.6	**0.5**
Cl	*ortho*	1.2	**0.7**
	meta	0.0	**0.0**
	para	0.1	**0.2**
Br	*ortho*	1.7	**1.1**
	meta	0.0	**0.0**
	para	0.0	**0.2**
		B6	
Cl	*cis*	0.0	**0.0**
	trans	0.5	**0.4**
Br	*cis*	0.0	**0.0**
	trans	–0.3	**0.1**

[a] The relative B3LYP/def2-TZVP energies at the PBE/def2-SVP geometry. [b] The relative Gibbs free energies (including ZPE and the $-RT \ln (q_{\mathrm{trans}}\, q_{\mathrm{rot}}\, q_{\mathrm{vib}})$ term) calculated at the PBE/def2-SVP level.

for the dihalogenated **B6** cages is 6:4 for the $B_6H_4Cl_2^{2-}$ and 1:10 for the $B_6H_4Br_2^{2-}$ compounds[45], which does not agree with the calculated thermodynamic stabilities. But again, the discrepancies are of the order of 1 kcal mol^{-1} (at this point, it should be repeated that equivalent thermodynamic stabilities or transition state barriers of the various positional isomers would lead to a 5:5:1 ratio between the *ortho*/*meta*/*para* isomers in the **B12** series and a 4:1 ratio between the *cis*/*trans* isomers in the **B6** series). To elaborate further on the positional preferences, we focus on the kinetic aspects.

*The Reaction Mechanism of the Halogenation Reactions on the **B12** Skeleton*

Experimental evidence. The halogenations (X = F, Cl, Br) of **B12** were carried out to an average presence of 1.0, 1.5 and 2 atoms of the halogen at the cage. The separation of monohalogenated derivatives and isomers of disubstituted derivatives is exemplified in the Experimental for the treatment of the mixture corresponding to a presence of 1.5 halogens. At this point, a mixture of the parent ion **B12**, $B_{12}H_{11}X^{2-}$, 1,7-$B_{12}H_{10}X_2^{2-}$ and 1,2-$B_{12}H_{10}X_2^{2-}$ (X = Cl, Br), along with only a small amount of trisubstituted (1,7,9-, 1,2,3- and other minor unidentified isomers) derivatives, arose as the products. Under the conditions described for fluorinations according to NMR, HPLC and MS evidence, a mixture of di- and trifluorinated $B_{12}H_{12}^{2-}$ anion formed, from which only 1,7-$B_{12}H_{10}F_2^{2-}$ could be isolated as a pure compound. The products were separated on DEAE cellulose and characterized by ^{11}B, ^{11}B-^{11}B COSY NMR spectroscopy and mass spectrometry (see Experimental). The *meta*/*ortho* isomer ratio was approximately 4:1 for chlorination and bromination.

*General theoretical considerations concerning the reaction mechanisms of the dihalogenation of **B12** and **B6** cages*. When conceiving reaction paths for the dihalogenation of **B12** and **B6** cages, we must bear in mind the fundamental differences in the chemistry of fluorine on one hand and chlorine and bromine on the other, as well as the differences in the chemistry of the **B12** and **B6** cages. Experimentally, the fluorination of **B12** is carried out using liquid anhydrous hydrogen fluoride (LAHF), whereas its chlorination and bromination are conducted using elemental Cl_2 or Br_2 in water (reviewed in ref.[6]). This is further complicated by the fact that Cl_2 or Br_2 can undergo disproportionation in water, yielding HX and HOX (X = Cl, Br) species, which in turn may dissociate and thus acidify the medium. The chemistry of **B6** is different in that the cage is easily disrupted in an acidic solution[7]. Thus, halogenation of **B6** with elemental Cl_2 or Br_2 proceeds in a strongly

basic aqueous solution[45]. In such a reaction mixture, X^-, OH^-, OX^- or HOX species can be present.

In the following sections, we will present the calculations of the reaction paths for the **B12** and **B6** cages: (i) the halogenation (X = F, Cl, Br) of **B12** and monosubstituted **B12** with HX **((***3a***)**, **(***3b***))** and X_2 **((***4a***)**, **(***4b***))** and (ii) the halogenation (X = Cl, Br) of **B6** and monosubstituted **B6** with HOX in the presence of hydroxide anions **((***5a***)**, **(***5b***))**.

$$B_{12}H_{12}^{2-} + HX \rightarrow B_{12}H_{11}X^{2-} + H_2 \qquad (3a)$$

$$B_{12}H_{11}X^{2-} + HX \rightarrow B_{12}H_{10}X_2^{2-} + H_2 \qquad (3b)$$

$$B_{12}H_{12}^{2-} + X_2 \rightarrow B_{12}H_{11}X^{2-} + HX \qquad (4a)$$

$$B_{12}H_{11}X^{2-} + X_2 \rightarrow B_{12}H_{10}X_2^{2-} + HX \qquad (4b)$$

$$B_6H_6^{2-} + HOX + \rightarrow B_6H_5X^{2-} + H_2O \qquad (5a)$$

$$B_6H_5X^{2-} + HOX + \rightarrow B_6H_4X_2^{2-} + H_2O \qquad (5b)$$

Halogenation of the **B12** Cage: A Direct HX Attack

The first reaction pathway studied was the direct attack of the HX molecule on **B12** boron cage. The reactants (**B12** and HX) form complexes where the positively charged hydrogen of the HX (X = F, Cl, Br) interacts via a dihydrogen bond[46] with the exoskeletal B–H bonds of the **B12** cages. This reaction complex leads to a transition state (TS), schematically illustrated in Fig. 2 (for the second halogenation step). The calculated activation barriers for the first halogenation steps are 66.3, 53.3 and 43.7 kcal mol^{-1} for X = F, Cl and Br. The reaction pathway continues directly to the products (monosubstituted **B12**) that are 14.7, 8.1 and 7.6 kcal mol^{-1} more stable than the reactants for X = F, Cl and Br, respectively. The second halogenation is characterized by a virtually identical reaction mechanism with the energy profiles depicted in Fig. 2. In the TS, the nascent B–X bond has a distance of 2.0, 2.7 and 3.0 Å for X = F, Cl and Br, respectively. Single imaginary vibration frequencies characterizing the TS were calculated as 1016i–1018i,

729i–792i and 588i–673i cm^{-1} for F-, Cl- and Br-substituted **B12**, respectively. The main components of the corresponding eigenvectors are along the axis of the formation of the B–X and H–H bonds of the products ($B_{12}H_{10}X_2^{2-}$ and H_2) and the breaking of the reactants' B–H and H–X bonds. The transition state barriers (relative to the isolated reactants, i.e. $B_{12}H_{11}X^{2-}$ + HX) are calculated as 62.2–63.5 kcal mol^{-1} for fluorination, 52.7–53.8 kcal mol^{-1} for chlorination, and 44.9–47.8 kcal mol^{-1} for bromination. Apart from fluorination, the smallest barrier is found for the disubstitution to the *meta* positions of **B12**. The released products are ~17, 11 and 10 kcal mol^{-1} more stable than the reactants for all the studied halogenations, respectively: therefore, the reaction is exothermic and exergonic with the *meta* isomers being energetically the most stable (as already discussed above) in all cases.

We can see that the directive effects of the first halogen substituent on **B12** for further halogenation are governed by both thermodynamic (cf. Table IV) and kinetic (Fig. 2) factors. However, it should be noted that in most cases the calculated energy differences are quite small and within the error bar of the methods used.

We can perceive, however, at least three problems in the studied reaction mechanism. First, the calculated data, unlike the experimental findings (it is known that only the reaction of **B12** with HF proceeds to a higher degree of substitution), suggest that the three studied reactions should be

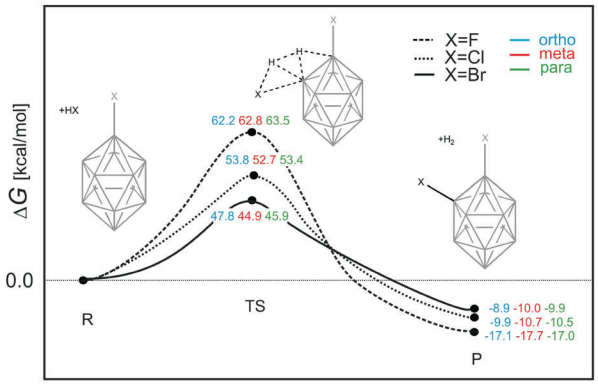

FIG. 2
The reaction pathway for the halogenation of monosubstituted **B12** with HX, X = F, Cl and Br (only shown for products in the *ortho* position; the *meta* and *para* disubstituted products are formed analogously). All the values were calculated at the B3LYP/def2-TZVP//PBE/def2-SVP level

kinetically preferred in the order F < Cl < Br. Second, both HCl and HBr are stronger acids than HF and only a fraction of the molecules exist in the HX state (with the rest being dissociated into H^+ and X^- species). Therefore, it is dubious to consider the presented mechanism for non-dissociated HX (X = Cl, Br) species, which have a very small concentration in solution. Third, it is known that chlorinations and brominations are carried out using X_2 as the reactant instead, and thus HX is present only as a fraction resulting from the disproportionation reaction and the reactive species is presumably the X_2 molecule. The last two phenomena led us to consider two other reaction mechanisms.

Halogenation of the **B12** Cage: An Acidic Mechanism

The alternative mechanism is expressed by the following equation:

$$B_{12}H_{12}^{2-} + HX \rightarrow B_{12}H_{12}^{2-} + H^+ + X^- \rightarrow B_{12}H_{13}^- + X^- \rightarrow$$

$$B_{12}H_{11}^- + H_2 + X^- \rightarrow B_{12}H_{11}X^{2-} + H_2 \,. \qquad (6)$$

The boron cage is first attacked by a proton from the HX acid, which, through a corresponding transition state, subsequently leads to H_2 elimination and, in the last step, the X^- anion is binding to the naked boron vertex. The ΔG value for the first step can easily be derived from the acidity constants of the halogen acids (pK_a = 3.1, –7.0 and –9.0 for X = F, Cl and Br, respectively, which corresponds to ΔG^0_{298} = +4.2, –9.6 and –12.3 kcal mol^{-1}). The calculated value for the protonation of the **B12** cage is 25 kcal mol^{-1} (assuming that the solvation energy of the proton is 264 kcal mol^{-1})[47]. Unfortunately, we were not able to converge the transition state structure corresponding to the H_2 elimination. Our best estimate for the activation barrier, based on the approximate TS, is 25 kcal mol^{-1}. According to our calculations, an approach of the X^- ion is then a barrierless process on the potential energy surface. Summing up these values, we obtain the following estimates of activation barriers: 53, 43 and 41 kcal mol^{-1} for X = F, Cl and Br, respectively. For chlorine, this barrier is quite similar to the reaction mechanism discussed in the previous section (a direct HX attack), whereas for fluorine, the barrier is ~10 kcal mol^{-1} lower. However, we have only repeated the previously calculated trends in the rate constants: F < Cl < Br, which is again in contrast with the experimental findings.

Halogenation of the **B12** Cage by X_2 Molecules

Finally, the chlorination and bromination of the **B12** cage using X_2 as the reactant is investigated. Both reactions are strongly exothermic and exergonic (ΔG^0 (ΔH^0) = –55.9 (–61.9) and –35.9 (–44.5) kcal mol^{-1} for X = Cl and Br, respectively). This causes the first halogenation step to be a transition state connecting the reactants and products with very small activation barriers of $\Delta G^{\#}$ = 0.1 and 8.7 kcal mol^{-1} for X = Cl and Br, respectively (the TS structures are similar to those depicted in Fig. 3 for the second halogenation step). This is in good agreement with the experimental finding that the chlorination reaction proceeds faster (this work and ref.[60]) and explains why both reactions are carried out at 0 °C (strong exothermicity). The transition state is characterized by an activation barrier of $\Delta E^{\#} \approx$ 6–10 kcal mol^{-1} on the PBE/def2-SVP potential energy surface (PES) and by the single imaginary frequency vibration (366i and 341i cm^{-1} for X = Cl and Br, respectively), connecting the reactants and products. This barrier is, however, reduced to almost zero on the B3LYP/def2-TZVP//PBE/def2-SVP PES as exemplified by the value of the free energy activation barrier presented above. The second halogenation step (Fig. 3) is characterized by the activation barriers of –0.5 to 5.3 kcal mol^{-1} for X = Cl and 8.8–12.9 kcal mol^{-1} for X = Br. Concerning the positional preferences, it was calculated that the *meta* and *para* positions are the kinetically preferred sites for the second halogenat-

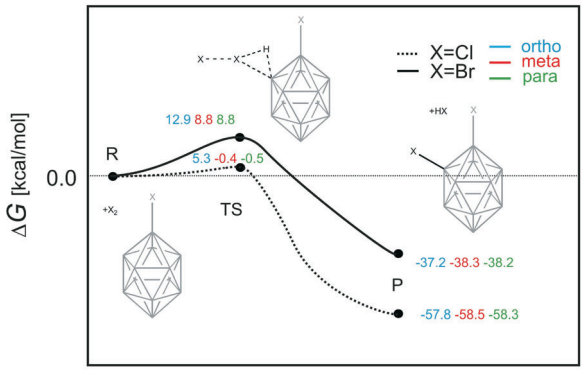

FIG. 3

The reaction pathway for the halogenation of monosubstituted **B12** with X_2, X = Cl and Br (only shown for products in the *ortho* position; the *meta* and *para* disubstituted products are formed analogously). All the values were calculated at the B3LYP/def2-TZVP//PBE/def2-SVP level. R, reactants; P, products; TS, transition state

ion. The former is in agreement with the experimental results, whereas in neither case (X = Cl, Br) we did reproduce the experimental finding that halogenation to the *ortho* position would be kinetically preferred to the *para* position. Nevertheless, both barriers are significantly smaller than the calculated barriers for the direct attack of HX, which suggests that we have found a plausible reaction mechanism for halogenation by the X_2 species for X = Cl and Br.

Halogenation of the **B6** Cage (Reactions (*5a*), (*5b*))

Since the $B_6H_4F_2^{2-}$ derivatives of **B6** had not so far been prepared experimentally, we have focused in our calculations on the chlorination and bromination reactions of **B6** only. We have found that the further halogenation of monohalogenated **B6** proceeds via a different pathway than that for **B12**, also because of the need for different experimental conditions, specifically the basicity of the solution[7]. The reaction mixture may be quite complex, containing X^-, OX^-, HOX and OH^- molecules. We, therefore, cannot be certain about the primary complexes of the reactants.

The sum of energies of the separated monosubstituted **B6**, X_2 and H_2O (Eqs (*5a*) and (*5b*)) species was set as a reference. The first barrier is connected with the formation of HOX and is ~10 kcal mol^{-1} higher for Br than for Cl (Fig. 4). The first step represents a **B6** cage opening brought about by

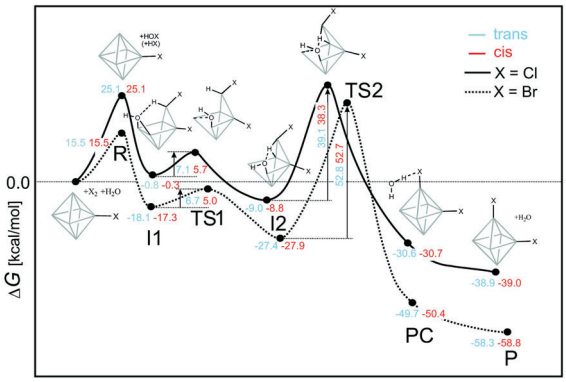

FIG. 4

The basic pathway for the halogenation of monohalogenated **B6** systems with HOX, X = Cl (· · ·) and X = Br (——) (only shown for products in the *cis* arrangement; the *trans* substitution proceeds analogously). R, reactants; I1 and I2, intermediates; TS1 and TS2, transition states; PC, product complexes; P, products

OH^- either alone or as a reactive group in the HOX moiety, leading to the first intermediate (I1). Energetically, I1 is stabilized by 17.3–18.1 kcal mol^{-1} for Cl and is approximately isoenergetic for Br, relative to the isolated reactant species (Fig. 4). I1 is characterized by the OH group bonding to a BB edge while the X moiety attacks the open BBB triangle. Overcoming a small barrier of 5.0–7.1 kcal mol^{-1} leads to a second intermediate (I2), stabilized by ~30 kcal mol^{-1} for Cl and ~10 kcal mol^{-1} for Br. The main feature of I2 is the disruption of the BB edge to which OH^- is attached. The rate-limiting step of the halogenation reaction of **B6** is the rearrangement to a second transition state (TS2) with a barrier of ~50 kcal mol^{-1} for Cl and ~40 kcal mol^{-1} for Br. The TS2 with a single imaginary frequency (908i and 1018i cm^{-1} for 1,2- and 1,6-$B_6H_4Cl_2^{2-}$, and 430i and 518i cm^{-1} for 1,2- and 1,6-$B_6H_4Br_2^{2-}$, respectively) shows both the recovered bonding of O(H) to the edge boron atom leading back to I2 and the formation of an O(H)–H bond, revealing the formation of the product water and disubstituted **B6** cage.

Comparing the chlorination and bromination pathways for monosubstituted **B6**, we observe in our calculations that the former has a smaller barrier (by approximately 10 kcal mol^{-1}) for the formation of the HOCl reactive species (which is in agreement with the experimental value of ~8 kcal mol^{-1})[48] but a ~13 kcal mol^{-1} higher barrier than the latter for the rate-limiting step. However, the overall activation barrier is ~26 kcal mol^{-1} for X = Cl and ~30 kcal mol^{-1} for X = Br. The chlorinated products are then ~20 kcal mol^{-1} more stable than the brominated ones.

DISCUSSION

*Calculated Structures and the ^{11}B NMR Chemical Shifts of the Parent and Substituted **B12** and **B6** Cages*

Standard quantum chemical tools, such as the second-order Møller–Plesset perturbation theory (MP2) and density functional theory (DFT) calculations, were often used in investigations of the structures, stabilities, reactions, interactions, and the ^{11}B NMR characteristics of boranes, heteroboranes, metallacarboranes and *exo*-substituted boranes[1,49–52]. Overall, the DFT or MP2 quantum chemical calculations were shown to be reliable enough to describe the above-mentioned phenomena and even make predictions. In this study, we follow this good performance by reproducing the X-ray structural data within a few pm and ^{11}B NMR chemical shifts mostly within 1–3 ppm (and at most by 5 ppm). As for the isomer preferences for

substitutions on cages, we show that thermodynamic stabilities are not sufficient to explain the experimental observations.

exo-Substituent Effects and Chemical Reactivity

B12 Cages

The first suggestions of the reaction mechanism were presented by Hoffmann and Lipscomb[53]. They assumed that the electrophilic substitution on **B12** by halogens would proceed to the adjacent boron positions 1,2 and 1,2,3 of the cage. However, the predictions for the directive effect of halogen on the cage were only marginally outlined in this paper, reflecting in the discussion that their calculations were performed only for +R, +I and –R, –I combinations of the inductive and resonance effects, whereas halogens show +R and –I effects instead.

The much later experimental work of Preetz et al.[54] seemed to indicate that this proposed path would be correct, reporting that the 1,2-isomer is the most abundant species resulting from a dihalogenation reaction of **B12**. This was undoubtedly based on misinterpretation of the ^{11}B NMR spectra, since the second isomer was not isolated and the data could not be compared. In contrast, our deeper experimental revision has proved unambiguously that the most abundant isomer is 1,7-$X_2B_{12}H_{10}^{2-}$ (X = Cl, Br). The 1,2-$X_2B_{12}H_{10}^{2-}$ isomer also arises in the reaction mixture, but only in a smaller ratio of ca. 20% according to the published HPLC analysis[17].

The NMR-based study was performed to understand the directive effect of a halogen substituent on a heteroborane cage towards further substitution[55]. The authors found that for SB_9H_9 and $SB_{11}H_{11}$ the sites of the initial attack do not correlate with the charge distribution on the cage and that the rearrangement of products is important. The same molecules were also studied theoretically, and the substitution preferences were explained in terms of occupied orbitals[56]. Regioselective fluorination was achieved for carborane clusters of varying size[57]. The DFT calculations showed that the isomer preferences are not controlled by relative stabilities but kinetically[58]. The reaction mechanisms of fluorination by HF of $CB_5H_6^-$ and $CB_9H_{10}^-$ carborane clusters were studied by McKee[34], who explained the experimentally observed isomer preferences on the basis of reaction barriers.

Based on our calculations, we have found the reaction pathway for the halogenation of the **B12** cage reminiscent of the electrophilic substitution mechanism for the $CB_{11}H_{12}^-$ carborane discussed by Michl et al.[59]. In short,

an HX molecule approaches the boron cage, forms a complex and via a transition state leads to the products through the release of the hydrogen molecule. The height of the calculated barriers suggests that the reaction rate should increase in the order F < Cl < Br. This is in contrast with the experimental finding of Muetterties et al.[60], who observed faster reaction kinetics for chlorination than bromination. In order to explicate this discrepancy further, we calculated the reaction barriers also for the first halogenation step (i.e. the monohalogenation of unsubstituted **B12**). Even here, the barriers decrease in the order F (~65 kcal mol^{-1}) > Cl (~53 kcal mol^{-1}). Therefore, this reaction mechanism seems to be unlikely. While the chlorination and bromination reactions are carried out using the X_2 species, we must admit that we do not currently have a plausible alternative for the fluorination of **B12** cages.

Concerning the isomer preferences, the calculated barriers to the formation of the disubstituted **B12** show preference for the *meta* isomer, which agrees with experimental observations (presented in this work). The experimentally observed ratio between 1,2-$B_{12}H_{10}Cl_2^{2-}$ and 1,7-$B_{12}H_{10}Cl_2^{2-}$ is approximately 1:4 (this work), which corresponds to the free energy difference of 0.8 kcal mol^{-1}. Thus, the calculated preference of the *meta* over *ortho* isomer in the transition state by 2.3 kcal mol^{-1} is in reasonable agreement with the experiment.

B6 Cages

Substitution chemistry on **B6** cages has been developed since the 1980s in the group led by Preetz[7,45]. Multiply (n = 2–6) halogenated species have been prepared for X = Cl, Br and I [45] but not for X = F [44]. The first substitution steps are rapid, whereas the continuation to perhalogenated **B6** cages is slower[45]. The obtained *cis*/*trans* ratios were approximately 6:4 for Cl and 1:10 for Br [45]. Our proposed cage-opening reaction mechanism (similar to that for the fluorination of $CB_5H_6^-$ found by McKee[34]) shows negligible difference (0.1 kcal mol^{-1}) in the free energy for the rate-limiting formation of the second transition state to yield the chlorinated isomers (Fig. 4), which agrees with nearly the same ratios of the isolated products. For bromination, the rate-limiting step for the formation of TS2 is 0.8 kcal mol^{-1} more favourable for the *cis* isomer, which is the opposite of what would have been expected based on experimental observation[48]. This discrepancy may be caused by the effects of spin-orbit coupling for the heavier Br, which were not included in our calculations of reaction barriers.

Based on the proposed reaction mechanism, we offer a plausible explanation for the difficulties in obtaining the $B_6H_4F_2^{2-}$ molecule experimentally. In the HOX series, HOF is chemically quite distinct from HOCl and HOBr (fluorine is negatively charged in $HO^{\delta+}F^{\delta-}$, whereas Cl and Br are positively charged in $HO^{\delta-}Cl^{\delta+}$, $HO^{\delta-}Br^{\delta+}$)[61]. The reactant would thus behave differently in the case of HOF.

Reaction Mechanisms on Borane Skeletons

A myriad of substitution mechanisms have been identified so far for the derivatization of boranes and carboranes[59]. For halogenation, electrophilic substitution (SE) and electrophile-induced nucleophilic substitution (EINS) mechanisms have been proposed. The latter was conceived to proceed via hydride abstraction and the subsequent attack of the nucleophile on the naked boron vertex. This mechanism may occur in experimental conditions where strong cations such as Li^+ are present. Here, we find rather the former mechanism for the halogenation of **B12**, where a transition-state complex is formed (Figs 2 and 3). For **B6**, the cage is first opened by a hydroxide anion and then the pathway proceeds via two transition states. Except for the presence of a hydroxide anion or HOX species, this mechanism is similar to that proposed by McKee for the fluorination of $CB_5H_6^-$ (ref.[34]).

The Relation to Substituted Benzene Molecules

Despite the similarity between the two classes of molecules with delocalized electronic distribution (two-dimensional, such as benzene, and three-dimensional, exemplified by octahedral and especially icosahedral boranes)[62], we confirm here that the directive effects in disubstitution are controlled by completely different chemistry. Recall that in the π-electron-rich benzene molecules, the first substituent causes a redistribution of electron density on the ring by the interplay of the inductive and resonance effects and thus controls the positions for further substitution[63]. The studied borane molecules differ from benzene in that the electrons delocalized over the cages are formally insufficient in numbers. Therefore, inductive and resonance effects are likely not to play such important roles as in the case of benzene molecules.

CONCLUSIONS

In this work, we have presented the results of an experimental and theoretical study of the exo-substituent effects in halogenations (X = F, Cl, Br) of icosahedral **B12** and octahedral **B6** cages. First, we show that calculations at the MP2 level with a double- or triple-ζ quality basis set describe the molecular structures of **B12** and **B6** clusters with sufficient accuracy. Specifically, the calculated equilibrium distances in *exo*-substituted **B12** and **B6** reproduce most X-ray crystallographic data to within 0.05 Å. Further, the calculations of ^{11}B NMR chemical shifts (magnetic shieldings) of *exo*-substituted **B12** and **B6** yield a very good agreement with the experiment (difference of 1–5 ppm). Second, we utilized DFT/B3LYP calculations to predict the thermodynamic stabilities of all the positional isomers of disubstituted **B12** and **B6** cages. We showed that the energy difference between the isomers is very small and that the regioselectivity of disubstitutions was not solely controlled by thermodynamic factors. Therefore, an attempt was made to address the kinetic aspects of these reactions by studying the relevant transition states and the associated energy barriers. Several pathways have been discussed with the aim of suggesting plausible reaction mechanisms and demonstrating the complexity of the chemical reactivity of boron cluster compounds. In general, reasonable agreement between the calculated activation barriers of the isomers of the disubstituted **B12** and **B6** systems and their experimentally observed preferences was found. We consider this work as our first attempt to study the reactivity of substituted borane and heteroborane compounds in a systematic way.

SUPPORTING INFORMATION

The equilibrium geometries of all the relevant transition states and Table S1 are available online (doi:10.1135/cccc2008189).

Some theoretical concepts and ideas presented in this work were initiated and formulated by Dr S. Heřmánek († 1999), our distinguished colleague, mentor and friend. We feel it appropriate to acknowledge his contribution by remembering that 'Art is longer than life'. We also thank Dr P. Cígler for fruitful and stimulating discussions on boron chemistry, to Mrs M. Kvíčalová for conducting the mass spectrometry measurements. The financial support of the Ministry of Education, Youth and Sports of the Czech Republic (LC523, LC512, Z40320502 and Z40550506), and the Grant Agency of the Academy of Sciences of the Czech Republic (40310613) is gratefully acknowledged.

REFERENCES

1. Schleyer P. v. R., Najafian K.: *Inorg. Chem.* **1998**, *37*, 3454.
2. a) Lipscomb W. N.: *Boron Hydrides*. W. A. Benjamin, Inc., New York, Amsterdam 1963; b) Williams R. E.: *Chem. Rev.* **1992**, *92*, 177.
3. Heřmánek S.: *Chem. Rev.* **1992**, *92*, 325.
4. a) Kutzelnigg W.: *Isr. J. Chem.* **1980**, *19*, 193; b) Schindler M., Kutzelnigg W.: *J. Chem. Phys.* **1982**, *76*, 1919; c) Kutzelnigg W., Schindler M., Fleischer U.: *NMR, Basic Principles and Progress*, p. 165. Springer Verlag, Berlin, Heidelberg 1990.
5. a) Onak T., Tseng J., Diaz M., Tran D., Arias J., Herera S., Brown D.: *Inorg. Chem.* **1993**, *32*, 487; b) Holub J., Jelínek T., Hnyk D., Plzák Z., Císařová I., Bakardjiev M., Štíbr B.: *Chem. Eur. J.* **2001**, *7*, 1546; c) Štíbr B., Tok O. L., Milius W., Bakardjiev M., Holub J., Hnyk D., Wrackmeyer B.: *Angew. Chem. Int. Ed.* **2002**, *41*, 2126; d) Bakardjiev M., Holub J., Hnyk D., Štíbr B.: *Chem. Eur. J.* **2008**, *14*, 6529.
6. Sivaev I. B., Bregadze V. I., Sjöberg S.: *Collect. Czech. Chem. Commun.* **2002**, *67*, 679.
7. Preetz W., Peters G.: *Eur. J. Inorg. Chem.* **1999**, 1831.
8. Muetterties E. L., Knoth W. H.: *Polyhedral Boranes*, Chap. 6, p. 103. Dekker, New York 1968; and references therein.
9. The *cis* and *trans* isomers of disubstituted **B6** can also be denoted as *exo* and *antipodal* (see, e.g., refs[7,45]).
10. Böhm S., Exner O.: *Pol. J. Chem.* **2007**, *81*, 993.
11. Böhm S., Parik P., Exner O.: *New J. Chem.* **2006**, *30*, 384.
12. Exner O., Böhm S.: *Curr. Org. Chem.* **2006**, *10*, 763.
13. Exner O., Böhm S.: *Collect. Czech. Chem. Commun.* **2006**, *71*, 1239.
14. Böhm S., Fiedler P., Exner O.: *New J. Chem.* **2004**, *28*, 67.
15. Domenicano A. in: *Stereochemical Applications of Gas Phase Electron Diffraction* (I. Hargittai and M. Hargittai, Eds), Part B, pp. 281–324. VCH Publishers, New York, Weinheim 1988.
16. Hnyk D., Holub J., Hofmann M., Schleyer P. v. R., Robertson H. E., Rankin D. W. H.: *J. Chem. Soc., Dalton Trans.* **2000**, 4617.
17. Grüner B., Plzák Z., Vinš I.: *J. Chromatogr.* **1991**, *588*, 201.
18. Ahlrichs R., Bär M., Häser M., Horn H., Kölmel C.: *Chem. Phys. Lett.* **1989**, *162*, 165.
19. Frisch M. J., Trucks G. W., Schlegel H. B., Scuseria G. E., Robb M. A., Cheeseman J. R., Montgomery J. A., Jr., Vreven T., Kudin K. N., Burant J. C., Millam J. M., Iyengar S. S., Tomasi J., Barone V., Mennucci B., Cossi M., Scalmani G., Rega N., Petersson G. A., Nakatsuji H., Hada M., Ehara M., Toyota K., Fukuda R., Hasegawa J., Ishida M., Nakajima T., Honda Y., Kitao O., Nakai H., Klene M., Li X., Knox J. E., Hratchian H. P., Cross J. B., Bakken V., Adamo C., Jaramillo J., Gomperts R., Stratmann R. E., Yazyev O., Austin A. J., Cammi R., Pomelli C., Ochterski J. W., Ayala P. Y., Morokuma K., Voth G. A., Salvador P., Dannenberg J. J., Zakrzewski V. G., Dapprich S., Daniels A. D., Strain M. C., Farkas O., Malick D. K., Rabuck A. D., Raghavachari K., Foresman J. B., Ortiz J. V., Cui Q., Baboul A. G., Clifford S., Cioslowski J., Stefanov B. B., Liu G., Liashenko A., Piskorz P., Komaromi I., Martin R. L., Fox D. J., Keith T., Al-Laham M. A., Peng C. Y., Nanayakkara A., Challacombe M., Gill P. M. W., Johnson B., Chen W., Wong M. W., Gonzalez C., Pople J. A.: *Gaussian 03*, revision C.02. Gaussian, Inc., Pittsburgh 2003.
20. Perdew J. P., Burke K., Ernzerhof M.: *Phys. Rev. Lett.* **1996**, *77*, 3865.

21. a) Becke A. D.: *Phys. Rev. A* **1988**, *38*, 3098; b) Lee C. T., Yang W. T., Parr R. G.: *Phys. Rev. B* **1988**, *37*, 785; c) Becke A. D.: *J. Chem. Phys.* **1993**, *98*, 5648; d) Stephens P. J., Devlin F. J., Chabalowski C. F., Frisch M. J.: *J. Phys. Chem.* **1994**, *98*, 11623.
22. Eichkorn K., Treutler O., Öhm H., Häser M., Ahlrichs R.: *Chem. Phys. Lett.* **1995**, *240*, 283.
23. Eichkorn K., Weigen F., Treutler O., Ahlrichs R.: *Theor. Chim. Acta* **1997**, *97*, 119.
24. Schäfer A., Horn H., Ahlrichs R.: *J. Chem. Phys.* **1992**, *97*, 2571.
25. Weigend F.: *Phys. Chem. Chem. Phys.* **2006**, *8*, 1057.
26. Weigend F., Ahlrichs R.: *Phys. Chem. Chem. Phys.* **2005**, *7*, 3297.
27. Klamt A., Schuurmann G.: *J. Chem. Soc., Perkin Trans. 2* **1993**, 799.
28. Schäfer A., Klamt A., Sattel D., Lohrenz J. C. W., Eckert F.: *Phys. Chem. Chem. Phys.* **2000**, *2*, 2187.
29. Lide D. R. (Ed.): *CRC Handbook of Chemistry and Physics*, 88th ed. CRC Press, Boca Raton 2007.
30. Jensen F.: *Introduction to Computational Chemistry*. John Wiley & Sons, New York 1999.
31. Kollwitz M., Gauss J.: *Chem. Phys. Lett.* **1996**, *260*, 639.
32. Ziegler T., Schreckenbach G.: *J. Phys. Chem.* **1995**, *99*, 606.
33. Onak T. P., Landesman H. L., Williams R. E., Shapiro I.: *J. Phys. Chem.* **1959**, *63*, 1533.
34. McKee M. L.: *Inorg. Chem.* **2001**, *40*, 5612.
35. Shoham G., Schomburg D., Lipscomb W. N.: *Cryst. Struct. Commun.* **1980**, *9*, 429.
36. Haeckel O., Preetz W. Z.: *Anorg. Allg. Chem.* **1995**, *621*, 1454.
37. a) Kuznetsov I. Yu., Vinitskii D. M., Solntsev K. A., Kuznetsov N. T., Butman L. A.: *Russ. J. Inorg. Chem.* **1987**, *32*, 3112; b) Zhukova N. A., Kuznetsov N. T., Solntsev K. A., Ustynok J. A., Grishin T. K.: *Russ. J. Inorg. Chem.* **1980**, *25*, 690.
38. A direct comparison of theoretical equilibrium distances with the experimental geometries should be made with caution, see, e.g.: Hargittai I., Hargittai M. in: *Molecular Structures and Energetics* (J. F. Liebman and A. Greenberg, Eds), Vol. 2, Chap. 1. VCH Publisher, New York 1987.
39. a) Solntsev K. A., Buslaev Yu. A., Kuznetsov N. T.: *Russ. J. Inorg. Chem.* **1986**, *31*, 633; b) Kuznetsov N. T., Solntsev K. A.: *Chemistry of Inorganic Hydrides*. Nauka Publ., Moscow 1990; c) Privalov V. I., Tarasov V. P., Meladze M. A., Vinitski D. M., Solntsev K. A., Kuznetsov N. T.: *Russ. J. Inorg. Chem.* **1989**, *34*, 630.
40. Macháček J., Plešek J., Holub J., Hnyk D., Všetečka V., Císařová I., Kaupp M., Štíbr B.: *Dalton Trans.* **2006**, 1024.
41. Grüner B.: *Ph.D. Thesis*. Czechoslovak Academy of Sciences, Prague 1990.
42. Grüner B., Heřmánek S., Plzák Z.: *Proceedings of the 7th International Meeting on Boron Chemistry – IMEBORON VII*, P. 5. Nicolaus Copernicus University Torun, Torun 1990.
43. Ivanov S. V., Lupinetti A. J., Solntsev K. A., Strauss S. H.: *J. Fluorine Chem.* **1998**, *89*, 65.
44. Thomsen H., Haeckel O., Krause U., Preetz W. Z.: *Anorg. Allg. Chem.* **1996**, *622*, 2061.
45. a) Fritze J., Preetz W., Marsmann H. C.: *Z. Naturforsch. B* **1987**, *42*, 287; b) Preetz W., Fritze J.: *Z. Naturforsch. B* **1987**, *42*, 282.
46. Custelcean R., Jackson J. E.: *Chem. Rev.* **2001**, *101*, 1963.
47. Tissandier M. D., Cowen K. A., Feng W. Y., Gundlach E., Cohen M. H., Earhart A. D., Coe J. V., Tuttle T. R., Jr.: *J. Phys. Chem. A* **1998**, *102*, 7787.
48. Greenwood N. N., Earnshaw A.: *Chemistry of Elements*. Pergamon Press Plc, Oxford 1984.
49. Bühl M., Holub J., Hnyk D., Macháček J.: *Organometallics* **2006**, *25*, 2173.
50. Fanfrlík J., Lepšík M., Horinek D., Havlas Z., Hobza P.: *ChemPhysChem* **2006**, *7*, 1100.

51. Fanfrlík J., Hnyk D., Lepšík M., Hobza P.: *Phys. Chem. Chem. Phys.* **2007**, *9*, 2085.
52. Fanfrlík J., Brynda J., Řezáč J., Hobza P. Lepšík M.: *J. Phys. Chem. B* **2008**, *112*, 15094.
53. Hoffmann R. L., Lipscomb W. N.: *J. Chem. Phys.* **1962**, *37*, 520.
54. Srebny H. G., Preetz W.: *Z. Naturforsch. B* **1984**, *39*, 189.
55. Smith W. L., Meneghelli B. J., Thompson D. A., Klymko P., McClure N., Bower M., Rudolph R. W.: *Inorg. Chem.* **1977**, *16*, 3008.
56. MacCurtain J., Brint P., Spalding T. R.: *J. Chem. Soc., Dalton Trans.* **1985**, 2591.
57. a) Ivanov S. V., Lupinetti A. J., Miller S. M., Anderson O. P., Solntsev K. A., Strauss S. H.: *Inorg. Chem.* **1995**, *34*, 6419; b) Ivanov S. V., Rockwell J. J., Miller S. M., Anderson O. P., Solntsev K. A., Strauss S. H.: *Inorg. Chem.* **1996**, *35*, 7882.
58. McLemore D. K., Dixon D. A., Strauss S. H.: *Inorg. Chim. Acta* **1999**, *294*, 193.
59. Körbe S., Schreiber P. J., Michl J.: *Chem. Rev.* **2006**, *106*, 5208.
60. Knoth W. H., Muetterties E. L., Miller H. C., Chia Y. T., Sauer J. C., Balthis J. H.: *Inorg. Chem.* **1964**, *3*, 159.
61. Srnec M., Ončák M., Zahradník R.: *J. Phys. Chem. A* **2008**, *112*, 3631.
62. King R. B.: *Chem. Rev.* **2001**, *101*, 1119.
63. McMurry J.: *Organic Chemistry*, 4th ed. Brooks/Cole Publishing Company, Pacific Grove 1996.